



Autonomous detection of calving-related seismicity at Kronebreen, Svalbard

A. Köhler¹, A. Chapuis², C. Nuth¹, J. Kohler³, and C. Weidle⁴

¹Department of Geosciences, University of Oslo, Norway

²Department of Mathematical Sciences and Technology, Norwegian University of Life Sciences, Norway

³Norwegian Polar Institute, Tromsø, Norway

⁴Department of Geosciences, Christian-Albrechts-Universität zu Kiel, Germany

Correspondence to: A. Köhler (andreas.kohler@geo.uio.no)

Received: 21 October 2011 – Published in The Cryosphere Discuss.: 2 December 2011

Revised: 21 March 2012 – Accepted: 22 March 2012 – Published: 30 March 2012

Abstract. We detect and cluster waveforms of seismic signals recorded close to the calving front of Kronebreen, Svalbard, to identify glacier-related seismic events and to investigate their relation to calving processes. Single-channel geophone data recorded over several months in 2009 and 2010 are combined with eleven days of direct visual observations of the glacier front. We apply a processing scheme which combines conventional seismic event detection using a sensitive trigger algorithm and unsupervised clustering of all detected signals based on their waveform characteristics by means of Self-Organizing Maps (SOMs). About 10% of the directly observed calving events close to the geophone (<1 km) can be correlated with seismic detections. We are able to distinguish between false detections, instrumental artifacts, and three classes of signals which are, with different degrees of uncertainty, emitted by calving or glacier activity in general. By extrapolating the interpretation of seismic event classes beyond the time period of visual observations, the temporal distribution of glacier-related events shows an increase in event rate in autumn, particularly for the class which is related to iceberg calving. Using the seismic event distribution in this class as a proxy for the calving rate and measurements of glacier velocity and glacier front position, we discuss the possible relationship between glacier dynamics and calving processes at Kronebreen.

therein), it is crucial to better understand the relationship between glacier dynamics and calving processes. Applying seismic observation and monitoring capabilities in glacier settings provides immense potential for this purpose (O’Neel et al., 2010; West et al., 2010).

Seismic recordings have been used to monitor dynamic glacial activity for about 30 or 40 yr (Vanwormer and Berg, 1973; Weaver and Malone, 1979; Wolf and Davies, 1986). Studies suggest different processes generating glacier-seismic events (glacier microseismicity), such as sliding at the base due to the glacial flow (Anandakrishnan and Bentley, 1993; Deichmann et al., 2000; Stuart et al., 2005), opening of cracks or crevasses (Blankenship et al., 1987; Deichmann et al., 2000), fluid-induced resonance (West et al., 2010), and calving. Calving events are often described as emergent low-frequency narrow-band (1–3 Hz) seismic signals (Qamar, 1988; O’Neel et al., 2007), and impulsive, high-frequency acoustic arrivals when measured close to the glacier front (Richardson et al., 2010). As sources, fluid-filled cracks and fracture processes before the calving (O’Neel and Pfeffer, 2007) or the detachment itself, followed by overturning and scraping of icebergs on the ocean seafloor (Amundson et al., 2008) have been suggested. Most studies recorded low-magnitude glacier events at local distances in the vicinity of the glacier, though moderate glacier earthquakes have been observed globally, for example, deriving from the outlet glaciers on Greenland and in Antarctica (Ekström et al., 2003; Nettles and Ekström, 2010). Furthermore, regional seismic networks have been shown to be capable of monitoring calving (O’Neel et al., 2010).

Iceberg calving is sporadic and therefore requires analysis of single-event data. A wide range of techniques can be applied to obtain data of single-event iceberg calving including time-lapse photography (Amundson et al., 2008), ground

1 Introduction

Iceberg calving is a key process of glacier dynamics which represents both a major uncertainty and a major contribution of ice mass to the oceans (Pfeffer et al., 2008). With increased observation of tidewater glaciers retreating, thinning and accelerating (e.g. Walsh et al., 2012, and references

based radar (Chapuis et al., 2010), and seismic/acoustic monitoring (O'Neel et al., 2007, 2010; Amundson et al., 2010; Richardson et al., 2010; Walter et al., 2010). However, a fully automatic method that provides inclusive information about the size, timing, type and location of iceberg calving events has yet to be developed. So far human-based perception has been used for various glaciers (e.g. Washburn, 1936; Warren et al., 1995; O'Neel et al., 2003, 2007) and is recognized as the “most practical method to acquire qualitative information about some calving processes” (van der Veen, 1997). However, this technique is practically limited to short observation periods due to the very intensive work in the field. It also contains some obvious problems related to lack of attention from the observers or limited visibility due to darkness or bad weather conditions that may reduce data quality.

The use of seismic data supplementary to direct (visual) monitoring of calving activity therefore opens the potential to match calving activity to seismicity and thus monitor calving autonomously (O'Neel et al., 2007). Once the relation and scaling between calving events and their seismic signals is understood, seismic records may improve the understanding of glacier calving and reveal variations in calving activity over longer time periods than monitoring through direct observations.

The objective of this study is to apply an autonomous seismic detection tool to geophone recordings at the front of a glacier over several summer months in order to monitor glacier calving. The study site for our experiment is Kronebreen ($78^{\circ}53' \text{ N}$, $12^{\circ}30' \text{ E}$), a grounded, polythermal tidewater glacier, located approximately 14 km south-east of Ny-Ålesund in western Spitsbergen (Fig. 1). Kronebreen is one of the fastest tidewater glaciers in Svalbard with an average front velocity ranging between 1 and 3.5 m per day during the summer months (Kääb et al., 2005; Rolstad and Norland, 2009) and with a terminal ice cliff having an elevation ranging from 5 to 60 m above the fjord surface at the end of August 2008 (Chapuis et al., 2010). We installed a geophone in the vicinity of the calving front from spring to autumn in 2009 and 2010 and collected ground-truth data of iceberg calving for 16 days by visual observations with an overlap of datasets of 11 days. We introduce a strategy to detect and cluster seismic events based on a STA/LTA trigger algorithm and an unsupervised learning method (Self-Organizing Maps). Seismic event clusters are then calibrated against the direct observations to extrapolate seismic signals due to calving activity beyond the ground-truth period. To assist analysis and interpretation of this geophone-calving timeseries, we compare it with the glacier velocity measured with GPS close to the front and changes in front position recorded by tracking the glacier terminus in terrestrial images.

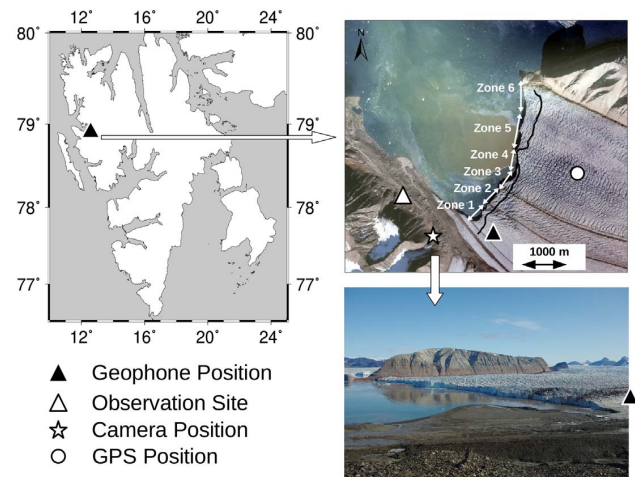


Fig. 1. Location of Kronebreen on Svalbard and position of instrumentation and observation site close to the calving front. Upper photo was taken in 1990 (Norwegian Polar Institute). Zones are indicated used to locate direct calving observations. Zone 6 comprises 700 m of the northernmost part of the glacier front, Zone 5 ranges from 700 to 1500 m, and Zone 1 to 4 are 500 m long each. Black line is front position on 29 August 2008. Lower photo shows view of glacier front as seen from the camera position close to the visual observation site in 2010.

2 Data

2.1 Seismic record

Several months of single-channel (vertical component) seismic data have been recorded on a PE-3 SM-4 geophone from 29 June to 15 August 2009, 11 September to 11 November 2009, and 8 May to 6 November 2010 with a sampling rate of 50 Hz. A Campbell CR1000 data logger recorded the raw voltage signal from the geophone which was sent to final storage through a serial cable to an Acumen compact flash memory module (because the Campbell data storage would not allow a full summer recording). This approach was restricted by transfer speed from the Campbell to the memory module which limited the amount of data we could record to 50 Hz rather than the ideal 100 Hz that is capable from the Campbell. Power supply was provided by a 12 V battery and a solar panel. In May of 2009 and 2010, the geophone was drilled 6 m into the ice and frozen into place. Melting during summer decreased the thickness of the overlaying ice layer to about 3 m. The position of the geophone (see Fig. 1), and therefore also the coupling with the ice, differ slightly between 2009 and 2010 since the instrument has been removed during the winter months. The analysis of the seismic record in this paper does not include location of events and a detailed investigation on their source mechanisms, as that would require more receivers, records of all three spatial wavefield components, and a sensitivity towards lower frequencies than the natural frequency of the geophone which is 10 Hz.

2.2 Direct calving observations

We monitored calving activity at Kronebreen based on human perception (viewing and hearing). Midnight sun in this region lasts from 18 April to 24 August which allowed continuous visual monitoring of the calving activity within our summer field excursions. Four people observed the calving front of Kronebreen during a total of 16 days split into two periods: from 14 August 2009 00:00 GMT to 26 August 2009 16:00 GMT and from 5 August 2010 23:30 to 15 August 2010 16:00. An overlap with seismic data of ~ 1.5 days in 2009 (477 observations) and 10 days in 2010 (2413 observations) is available for matching calving events to seismic detections. The camp from which we observed the glacier front was located approximately 1.5 km west of the front, which provided good coverage of the front. We estimated that $\sim 90\%$ of the front was visible for the observers (see Fig. 1).

For each calving event within the period of visual observation we registered the time (to a relative accuracy of 10 s), style, location and size. The style of iceberg characterizes the type of calving event. We follow the O'Neel et al. (2003) classification into 6 classes: avalanches, block slumps, column drops, column rotations, submarine and internal. Avalanches and block slumps affect only parts of the glacier front, block slumps being bigger than avalanches. Column drops affect the entire subaerial part of the ice front which collapses vertically. Column rotations collapse with a rotation movement and can affect the subaerial part of the ice front alone or the entire ice wall, submarine part included. Submarine events are icebergs being detached from the ice front below the water line. The last type of event is internal and refers to either very small calving events that we could not visually observe or ice blocks falling into crevasses. In both cases they are related to glacial activity close to the front.

We also visually estimated a size for each event, which reflects the volume of ice detached from the front during a calving event. It allows a semi-quantitative approach as first introduced by Warren et al. (1995). The size scale repeats the one defined by O'Neel et al. (2003) but we extended it from 1 to 20, 20 being the entire front width collapsing. We estimated the error on the size scale caused by the subjectivity of the observers to be ± 1 based on common observation periods where we compared the size each observer gave for a set of training events. This size scale is an indirect measure of iceberg volume, where Size 1 is about 10 m^3 and Size 4 about 1000 m^3 (Chapuis, 2011; Chapuis and Tetzlaff, 2012). Each event is classified into 6 zones along the 3.5 km front, Zone 1 being closest to the observation site and geophone installation (Fig. 1). For a detailed description and discussion of this direct observational dataset, we refer to Chapuis and Tetzlaff (2012) and Chapuis (2011).

2.3 Glacier velocity from GPS measurements

Glacier velocity is measured using a single code based GPS receiver approximately 2 km from the front position. The instrument is an IMAU construction (Den Ouden et al., 2010) that records one measurement every hour which is sent through ARGOS to the base server. Velocity is determined through a variety of filtering techniques based upon the number of days of smoothing. Here, we use an average of 3 days.

2.4 Front position from terrestrial photogrammetry

Repeat photographs were taken every hour from the same location (star in Fig. 1) using Harbotronics time-lapse cameras (e.g. Chapuis et al., 2010). Weekly pictures are used to track the front position. The position of the camera does not allow for accurate, absolute measurements of front position changes. However, simple image to image comparison using stable reference points provides relative frontal change as estimated by cumulating binaries (+1 for advance, -1 for retreat). This results in a non-scaled timeseries of retreat/advance relevant for analyzing our seismic-calving proxy. Photographs cover the entire seismic record from 9 May 2009 until 29 September 2009 and from 16 April 2010 until 13 November 2010. Details on the acquisition systems and methods are described in Chapuis et al. (2010).

3 Method

Conventional automatic event detection in seismology is usually done using Short Time Average over Long Time Average (STA/LTA) trigger algorithms which report distinct signal arrivals when amplitudes exceed the background noise level, but generally do not distinguish between (i.e. classify) different kind of events. In order to achieve a more precise classification and to handle the large amount of available data, making use of automatic pattern recognition techniques is therefore becoming increasingly important in seismological studies. Supervised classification algorithms can be employed to detect seismic events based on manually prepared training data sets (e.g. Joswig, 1990; Dowla et al., 1990). On the other hand, unsupervised pattern recognition may be used to generate an initial understanding of the unknown data properties without utilizing existing class or event labels as done for supervised learning (Bardainne et al., 2006; Köhler et al., 2009). Clustering is a well-known unsupervised learning method which describes the task to find a meaningful grouping of unlabeled data into respective categories (e.g. Jain, 2010).

When it comes to autonomous detection of seismic signals for glacier monitoring, STA/LTA methods are commonly applied (e.g. Amundson et al., 2010). Since different types of glacier-generated signals (e.g. due to calving and fracturing) have been found to have different spectral characteristics, frequency domain processing can be used to

classify detected events (O'Neel et al., 2007, 2010; West et al., 2010), which particularly benefits from the narrow-band character of calving-related seismic signals. A disadvantage of STA/LTA trigger algorithms might be that emergent signal onsets may be missed which are typical for calving. O'Neel et al. (2007) therefore suggested a method which performs both the detection as well as the classification in the frequency domain. Detection and classification parameters (thresholds) were found in a supervised manner by using direct calving observations as ground-truth data for training.

Here, we present and apply a processing scheme to detect and identify glacier-seismic signals which combines event detection using a STA/LTA trigger and (unsupervised) clustering. While the trigger algorithm will automatically detect all sorts of seismic events in the data, clustering detections into groups with similar signal characteristics helps to distinguish different types of seismic events and false alarms. This approach is suitable and reasonable for our purpose, since no detailed information about the character of potentially observable glacier-seismic signals at Kronebreen was available a priori. Our approach is similar to the one used by West et al. (2010). In that study glacier-related seismic events have also been detected using a STA/LTA trigger and then analyzed with respect to the existence of groups of similar signals. Our study uses automatic clustering for the latter step, rather than using a manual statistical analysis.

3.1 Seismic event detection

We use a modified version of the STA/LTA trigger function introduced by Allen (1978) which also provides an estimate for the end time of the event (STA function falls below a certain threshold for a defined number of time steps). We calibrate the algorithm parameters based on visual assessment of identified events in selected time windows. A STA window length of 0.4 s, a LTA window length of 3.5 s, and a STA/LTA threshold of 3 are chosen (other parameter: $C_2 = 3$, see Allen, 1978). This parameter setting makes the detection algorithm very sensitive to catch all event types, including short and weak ones, to obtain a catalog of glacier-related seismicity as complete as possible. The low STA/LTA threshold will also increase the probability that emergent signals are triggered. A drawback of such sensitivity is that the algorithm results in many false detections. We deal with this problem in the second phase of our approach. Note that West et al. (2010) used a larger STA/LTA threshold of 10 to keep high quality events only (and to avoid false detections) at this stage.

3.2 Seismic event clustering

Although clustering is considered an unsupervised process (i.e. grouping of data itself is fully automatic), human interaction is an integral part. Choosing a meaningful number of clusters, validating and interpreting the results are crucial

steps which must be accomplished by the analyst. Most algorithms generate a cluster solution for a fixed number of clusters and have, therefore, to be tested using different values. Furthermore, cluster validation requires an assessment whether the clustering solution is in fact a good representation of the natural grouping of the data set. In order to select the most meaningful solution, quantitative approaches can be used to compute a measure for the cluster validity, e.g. the Davies Bouldin index (DB, Davies and Bouldin, 1979). However, there is often not a single best solution and validity measures may not result in the most meaningful grouping. Visualization of clustering solutions, which must be useful also for multi-dimensional data, is one way to solve this problem (Vesanto and Alhoniemi, 2000). Finally, once a cluster solution has been found representing the natural grouping of the data, the meaning of clusters has to be determined based on expert knowledge, e.g. by considering examples or a generalized pattern from each cluster. Within this process, it might become necessary to choose another cluster solution or split and merge individual clusters.

We apply the Self-Organizing Map (SOM) technique, a quasi-artificial, unsupervised neural network used to intuitively visualize and cluster multidimensional data (Kohonen, 2001), which has been successfully applied for pattern recognition in seismology (Maurer et al., 1992; Musil and Plešinger, 1996; Tarvainen, 1999; Plešinger et al., 2000; Esposito et al., 2008; Köhler et al., 2010). The main property of SOMs is that data can be mapped on a two-dimensional, regular grid of usually hexagonal SOM units. This mapping is ordered and topology-preserving, meaning that close or similar data vectors in the input space are also close on the SOM. In that way one can visualize the distribution of multidimensional data in two dimensions, so that location of data projected on the SOM reflects the natural data grouping in the input space. As a final step, the SOM units can be grouped automatically using common clustering methods. For more details about the SOM method see Kohonen (2001). Examples and more detailed description of SOM clustering and visualization can be found e.g. in Köhler et al. (2009, 2010).

In order to cluster a set of detected seismic events, a set of discriminative features is required for each detection which form the input data vector. West et al. (2010) showed that the dominant frequency of a detection can be used as a single feature in case of seismic broadband recordings to distinguish, in their case, two populations of glacier-seismic signals. However, the bandwidth of our instrument is not sufficient to compute a broadband seismic spectrum (i.e. lack of sensitivity below 10 Hz, flat response above) and therefore other features are needed in addition to characterize an event. Furthermore, the idea of unsupervised learning is to find clusters that may not have been identified manually by the analyst in advance. Therefore, the use of several features increases the probability to discover more existing classes. We want to point out that a simple classifier (e.g. based on a single feature) can still be an effective detection

method once a clear class of seismic signals of interest has been identified. Here, we choose features that are potentially suitable to distinguish waveforms of different event types and false detections. These features are based on statistics on the seismogram amplitudes, the frequency spectrum, and temporal characteristics of an event (Fig. 2):

- Number of Runs (per sample): the number of runs is based on a significance test (Runs Test) for temporal randomness which evaluates whether all samples of a sequence are mutually independent (Wald and Wolfowitz, 1940; Köhler et al., 2009). A run of a time series is a sequence of adjacent samples below or above the mean, i.e. a white noise time series would have a high number of runs since the amplitude varies randomly around the mean over time. A seismic event on the other hand would have a lower number of runs. The seismogram time window considered to compute the number of runs begins 20 s before the event onset and ends 20 s after the event stopped according to the estimate made by the trigger function. The number of runs is computed from the seismogram envelope and is normalized with the number of samples in the time window. The envelope is computed from the analytic (complex) seismogram (Taner et al., 1979).
- Spectral Ratio: the frequency spectrum is computed from the detected signal only (no temporal context). The ratio of mean spectral amplitudes between 12 and 19 Hz and 0.5 to 25 Hz is computed to account for different frequency content of seismic signals. Other spectral ratios have been tested, but the chosen one had the best discrimination ability.
- SNR: the Signal to Noise ratio is computed as the logarithmized ratio of the RMS (root mean square) of the event amplitudes and the RMS of the time window before the event which has the same length as the event. The SNR can be useful to identify false detections.
- Length: the duration of the event in seconds is obtained from the STA/LTA trigger. The length has been shown to differ for various types of glacier-related seismic events.
- Standard deviation: see skewness.
- Skewness: standard deviation and skewness are computed from the signal envelope to describe its shape. The same time window as for the number of runs is used. Both features are normalized with the mean of the envelope.

4 SOM training and cluster definition

The STA/LTA trigger generates 24 278 detections for the entire seismic record, including an unknown amount of false

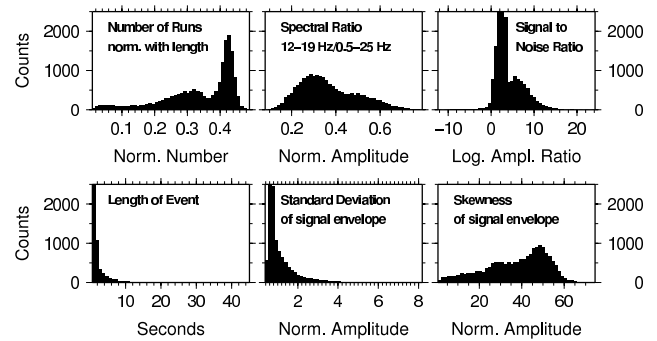


Fig. 2. Distribution of features forming input data vectors for clustering computed for all detected seismic events. Bimodal distributions denote existence of clusters.

detections. We use all detections to generate the SOM input data set by computing the characteristics introduced above from each signal. The frequency distribution of each feature in Fig. 2 reveals that at least two distinguishable classes are present in the data set, since some features show a clear bimodal distribution (West et al., 2010).

The SOM generation or training is an iterative process of finding representative data vectors associated with each SOM grid unit (Kohonen, 2001). After training, the SOM is clustered using an average linkage hierarchical clustering algorithm (Vesanto and Alhoniemi, 2000). Cluster solutions from 2 to 35 clusters are generated. The best solution is defined manually using the DB index as a guideline and evaluating the so-called unified distance matrix plot of the SOM (U-matrix, Fig. 3a) which illustrates the probability density distribution of data vectors (Vesanto and Alhoniemi, 2000). Comparison of the clustered SOM (Fig. 3b) and the U-matrix allows for the validation of clusterings. For a perfect grouping, cluster borders should appear as more reddish (less-dense) areas in the U-matrix plot in comparison to the regions inside the clusters. In other words, a cluster is a bounded, blue area on the SOM. We correct the number of clusters obtained from one good solution (low DB index) by splitting individual clusters based on the hierarchical cluster solution (grey clusters in Fig. 3b), resulting in 25 clusters.

5 Results and discussion

5.1 Classification based on direct observations

The cluster solution in Fig. 3b represents the grouping of seismic detections in the feature space. However, in order to identify the meaning of each cluster, ground-truth data is required to match known event types to their corresponding clusters. Furthermore, we have to inspect detection examples from each cluster and decide what sort of signals is present based on seismological expertise. Due to the lack

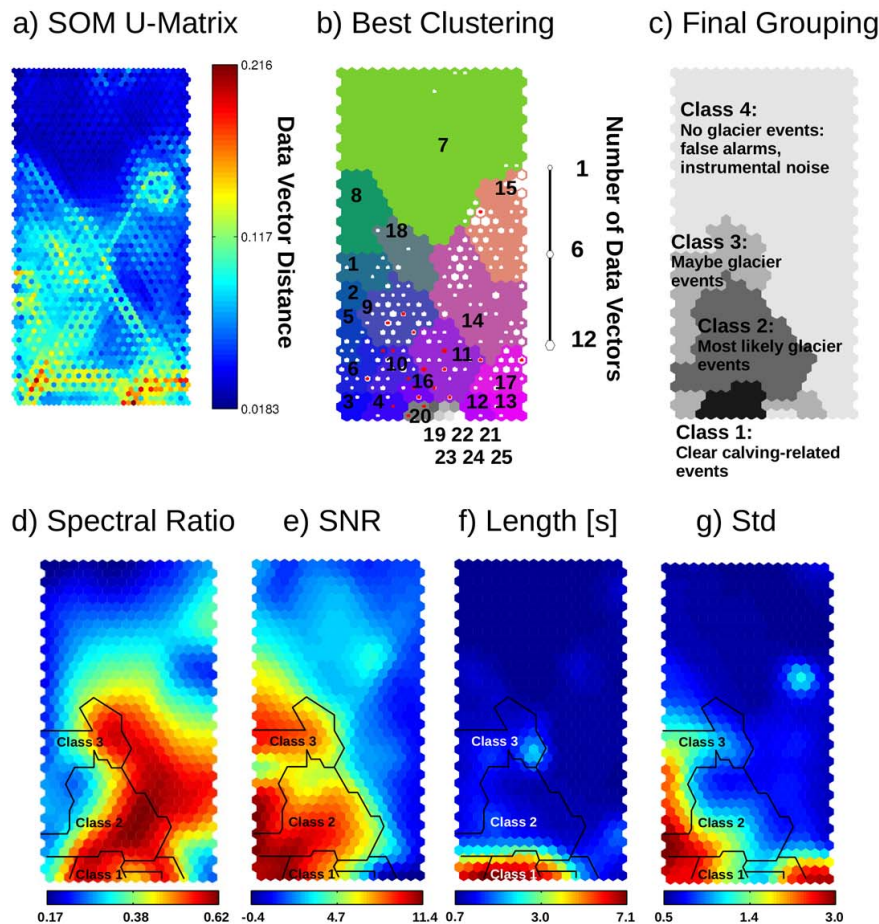


Fig. 3. SOM and clustering of detected seismic events. **(a)** Unified distance matrix (U-matrix) which reveals data density in input space. Each SOM unit is divided into seven sub-unit. Each sub-unit is colored according to distance between corresponding data vectors of neighbor units. Areas with low distances (blue) indicate high data density (i.e. clusters). **(b)** Cluster solution chosen based on U-matrix and DB index (see text). Cluster membership of each SOM unit is indicated by color. Clusters with a grey scale fill are those which are obtained by splitting clusters from one solution with 18 clusters. Symbols show data projected on SOM. Sizes of hexagons correspond to number of projected data vectors represented by a SOM unit. White symbols correspond to detections within 11 days long period where direct observations of glacier front are available (matched and unmatched). Red symbols are detections matching with events observed in Zone 1. **(c)** Final grouping of events based on matching rates and inspection of examples from each cluster. **(d–g)** Component planes for four selected features: Ratio between mean spectral amplitudes, signal to noise ratio, length of a detections, and standard deviation of signal envelope. Each SOM unit is colored according to value of a particular data vector component. Red colors stand for high values of corresponding feature. Outline of signal classes is indicated.

of man-made noise in the remote study area, we can assume that most detected seismic events are related to natural (e.g. glacial) activity.

First, all detected seismic signals are identified during the period of direct observations, in which 98 (2009) and 238 (2010) detections are obtained (white symbols on the SOM in Fig. 3b). We then match these seismic detections with directly observed calving events at the glacier front (see Fig. 4). We choose a 40 s long time window (± 20 s from start of a detection) to find calving events which could be related to a particular seismic event. Table 1 presents a summary of the results for the different types, locations, and sizes of visually observed calving events.

In order to evaluate the resulting recognition rates and to exclude random matches, we apply a binomial test for statistical significance (Table 1). The probability is computed that a number of x random matches is produced after a number of N trials corresponding to the number of direct observations and a matching probability of p , where p is the ratio of number of seismic detections and number of 40 s long time windows within period of direct observations. Results show that the matches for Zone 2, 3, 4, and 6 can be explained by a number obtained by chance assuming a significance level of 5% for passing the test for randomness. Only results for Zone 1 and 5 cannot be explained by random matches. However, only calving observations in Zone 1,

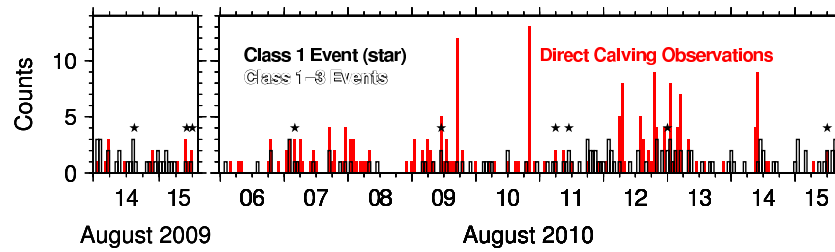


Fig. 4. Temporal distribution of direct (visual) calving observations and Class 1–3 seismic events within calibration period in 2009 and 2010.

Table 1. Results of matching seismic detections and visually observed calving events for 11 days. “All” means that all observations are used including a number of 101 not assigned to one of the 6 zones. “Matching Rate” is percentage of visual observations that can be related to seismic detections. “Significance Random Match” refers to binomial test for statistical significance of matches. It is probability that matches can be produced by chance.

Calving Events	Visual Observations	Seismic Matches	Matching Rate	Significance Random Match
All	2890	67	2.3 %	0 %
Zone 1	222	20	9.0 %	0 %
Zone 2	709	10	1.4 %	12.6 %
Zone 3	488	6	1.2 %	15.5 %
Zone 4	717	11	1.5 %	11.3 %
Zone 5	469	13	2.8 %	0.8 %
Zone 6	184	4	2.2 %	13.7 %
Zone 1 avalanches	18	0	0 %	77.9 %
Zone 1 block slumps	39	5	12.8 %	0 %
Zone 1 column drops	17	2	11.8 %	2.1 %
Zone 1 column rotations	6	1	16.7 %	7.7 %
Zone 1 submarine	2	0	0 %	97.3 %
Zone 1 internal	140	12	8.6 %	0 %
Zone 1 Size 1	148	11	7.4 %	0 %
Zone 1 Size 2	43	5	11.6 %	0 %
Zone 1 Size 3	25	4	16 %	0 %
Zone 1 Size > 3	6	0	0 %	92.0 %

which is the closest to the geophone, are recognized as seismic events with a rate of 9 %, which is clearly higher than for the other zones. The rates are even higher when we only consider block slumps and column drops in Zone 1. For column rotations and submarine events, too few observations are present to obtain a reliable statistic. However, it seems that avalanches do not emit clear seismic signals strong enough within the sensitive frequency band to be recorded by the geophone. Furthermore, Table 1 shows that the recognition rate increases with size of the observed calving. It is largest (16 %) for events of Size 3. It is intuitively clear that more of the closest and largest calving events observed at Kronebreen are detectable (i.e. Size 3), since amplitudes of seismic waves are attenuated as a function of distance and the detection threshold is limited by the noise level in the seismic data. Even though we obviously are not able to monitor seismic

emissions from the entire glacier front, we can proceed with investigating the subset which we are able to detect. We cannot exclude that we also observe events from the other zones (e.g. Zone 5), however, the evidence is strong enough that we indeed can see calving events from Zone 1.

The matching rates in Table 1 have been computed using all detections and are not based on specific clusters. However, we are now able to identify individual event clusters considering the detections matching with Zone 1 events. The red symbols in Fig. 3b represent the matching detections in the SOM space and are clearly confined to the lower part of the map. Hence, clusters located within that area are most likely glacier-event classes (e.g. iceberg calving). Some clusters do not include matches with direct observations, but the corresponding detections are clear seismic events. Furthermore, there are transition clusters where it is not clear

whether the corresponding detection are instrument artifacts or very short and weak seismic events. Those clusters are not labeled as event clusters. To simplify the following discussion, we reduce the obtained clusters to four classes with similar percentages of matched detections (Zone 1) within a cluster and similar distribution of features on the SOM (Table 2 and Fig. 3c). Hence, those classes reflect the uncertainty of whether signals are related to the calving process as well as the character of its signal (see Figs. 3, 4 and 5). The classes are:

- Class 1: clear glacier-seismic events related to calving (> 30 % matched within cluster).
- Class 2: most likely glacier-seismic events (> 5 % and < 30 % could be matched).
- Class 3: maybe glacier-seismic events (no matches, but clearly no false detections).
- Class 4: no glacier-seismic event (instrument artifacts and triggered background noise fluctuations).

Two matches with Zone 1 events (from 20 in total) are clearly identified as false detections (Class 4) which matched by chance (see Fig. 3b and Table 2). For the other locations, the fraction of Class 4 events among all matches is significantly higher, what confirms our hypothesis that these matches are produced by coincidence for the most part (6 of 10 for Zone 2, 5 of 6 for Zone 3, 6 of 11 for Zone 4, 11 of 13 for Zone 5, 4 of 4 for Zone 6).

5.2 Seismic signal characteristics

In order to investigate the meaning of clusters, SOM component plane plots are useful for displaying the feature distribution or values of a particular data vector component which is associated with any of the SOM units. A selection of SOM component planes (Fig. 3d–g) and randomly selected examples of seismic waveforms (Fig. 5) shows the different characteristics of each event class. As expected, all event clusters (Class 1 to 3) are characterized by higher signal to noise ratios (SNR) compared to the rest of detections (Fig. 3e). Class 1, which is related to iceberg calving, consists of rather long events, typically 4–10 s (see Fig. 3f), with several signal arrivals (local amplitude maxima, Fig. 5). Very short, impulsive signals seem to be characteristic of Class 2 (0.5–1 s).

Full spectral resolution is limited to frequencies larger than 10 Hz. However, we can still observe different characters of the frequency spectrum from the spectral ratio feature in Fig. 3d, where high values indicate a larger contribution of higher frequencies. Parts of Class 2 (mainly Cluster 10 and 11) show slightly higher values than Class 1. In fact, considering individual frequency spectra clearly showed that Class 1 has amplitudes peaks between 5 and 15 Hz, whereas in Cluster 10 and 11 events (Class 2) spectral amplitudes

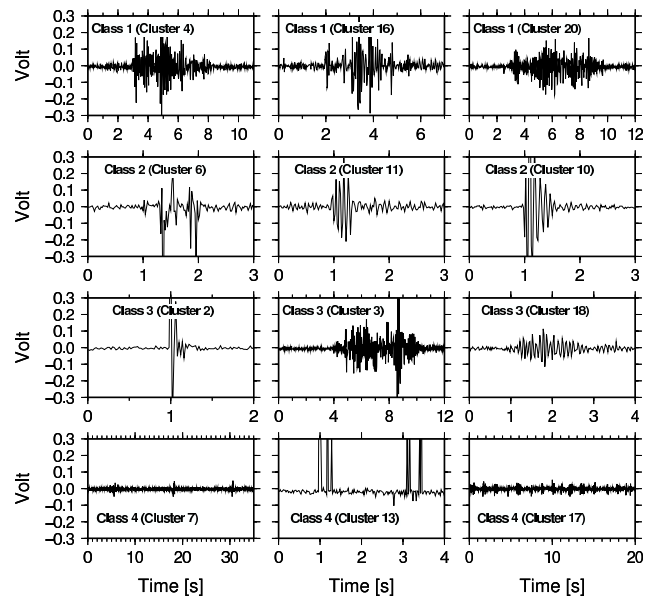


Fig. 5. Randomly selected examples of all event classes. Class 1: clear calving-related seismic events, Class 2: most likely glacier events, Class 3: maybe glacier events, Class 4: no glacier events. Same amplitude scale for all classes.

dominate between 10 and 20 Hz. The fact that we still observe contribution between 5 and 10 Hz for Class 1, despite of the decaying instrument sensitivity, shows that the main spectral content is probably localized at lower frequencies. However, why do parts of Class 2 and Class 3 (left hand-side of the SOM) and almost all detections of Class 4 have very low spectral ratios? The apparent contribution of very low frequencies (0.5–5 Hz) below the sensitivity limit of the geophone is a result of amplitude spikes, most likely instrument artifacts, which we were not able to remove completely with a despiking algorithm. Those amplitude peaks are quasi delta functions and therefore include all frequencies. Another indicator of high amplitude peaks are high values for the standard deviation feature (Fig. 3g). On the other hand, a cigar-shaped envelope (see Cluster 18 event in Fig. 5) will have a low standard deviation. Class 3, which was defined as the event group which could not be correlated with calving events, shows characteristics of Class 1 as well as Class 2 events (Fig. 5). Figure 3d and g shows that those events cluster into different groups mainly because they are contaminated by spikes.

We do not observe typical seismic signals with clearly separated P and S-Wave onsets in accordance to observations made by Amundson et al. (2010) and O’Neel et al. (2010). The complexity of waveforms, especially those of Class 1 (Fig. 5), could reflect the nature of a calving event, which is rather a sequence of events than a signal from a single, shortly acting source. It is also possible that we observe parts of the acoustic signal of an event coupled with the ice surface in addition to direct seismic waves (Richardson et al., 2010).

Table 2. Event classes obtained from clustering and defined based on matching seismic detections and visual observations. Class 1: clear glacier events related to calving, Class 2: most likely glacier events, Class 3: maybe glacier events, Class 4: no glacier events. “Detections in Matching period” is the number of seismic detections during the matching/ground-truth period. “Matches Zone 1” is number (and percentage) of seismic detections which can be related to a direct observation in Zone 1. “All detections” refers to seismic detection within entire time of seismic recording in 2009 and 2010. The last column states the clusters merged to define classes (see Fig. 3b, c).

Class label	Detections in Matching Period	Matches Zone 1	All Detections	Clusters
1	9	5 (56.6 %)	792	4, 16, 20
2	107	13 (12.2 %)	3699	6, 9, 10, 11
3	22	0	3359	1–3, 5, 12, 18, 19, 21, 22
4	200	2 (1 %)	16 428	7, 8, 13–15, 17, 23–25

Two different general types of glacier-related seismic events close to the terminus, measured at local distances as in our study (i.e. several kilometers from terminus), have been consistently observed by several studies at the Columbia glacier, Alaska (Qamar, 1988; O’Neel et al., 2007; Walter et al., 2010) and on Greenland (Amundson et al., 2010). Emergent, 2 s to several minutes long signals have been related to directly observed iceberg calving. These events are narrow-band between 1–3 Hz and may be related to fluid resonance and/or a common small fault size (O’Neel et al., 2007). Types of signals with similar characteristics have been observed by Amundson et al. (2010), who found events with frequency content of 4–6 Hz related to avalanching ice, and also Richardson et al. (2010). The second type of signals are shorter, 0.1 to 5 s long impulsive seismic events with energy at higher frequencies (10–20 Hz or 6–9 Hz), which have been interpreted as being generated by crevassing.

Considering event duration and frequency content, Class 2 events in our study are very similar to the second class of signals and may therefore be interpreted as due to ice fracturing. Class 1 shares similarities in length and frequency content relative to Class 2 with the first-mentioned type of longer seismic events which have been observed at lower frequencies in combination with calving. This supports our interpretation that Class 1 is directly related to calving. However, since we may not see the main energy contribution below 10 Hz (O’Neel et al., 2007, 2010) due to the instrument sensitivity as discussed above, some uncertainties remain. The fact that this type of seismic calving event is commonly observed in a narrow band at low frequencies may also explain why we detect directly observed calving with only a success rate of 10 %. We may only speculate that the relatively low success rate has to do with the lower observed frequency (1–3 Hz) of calving seismic signals observed in other parts of the world in combination with the low sensitivity of the geophone at these frequencies.

5.3 Extrapolation of calving rate beyond calibration period

Within the time period of direct observations, we have good indications that 138 detections belonging to Class 1, 2, and 3 can be interpreted as glacier-seismic events and that Class 1 is most likely related to iceberg calving. This interpretation is based on seismic signal characteristics as well as on matching with direct observations. We have to make two assumptions if we want to extrapolate the event rate of Class 1 as a proxy for the calving rate beyond the calibration period. First, there should be no other dominant process at the glacier that generates Class 1 events in the calibration period and behaves independently from calving over time (e.g. basal sliding, fracturing). We have to consider this possibility since about 43 % of the Class 1 events do not exhibit matches with directly observed calving (Table 2). Secondly, even if all Class 1 events are generated by calving in the calibration period, there could be another process which is not active in the calibration period and generates Class 1 events at another time. Furthermore, we have to be aware of the fact that the event rate of Class 1, if it represents calving, is only valid for Zone 1 close to the measurement site and most likely underestimates the real rate due to the limited instrumental sensitivity as discussed above.

Different glacial processes have been shown to emit signals with different characteristics as discussed above. Therefore, the clustering which we performed should be able to distinguish between those processes. Furthermore, when we assess similarity of seismic events on a more detailed level and consider sub-clusters of Class 1, i.e. divide the class into the hexagonal SOM units (see Fig. 3) and consider the associated seismic detection, we observe the same temporal patterns as for all events in Class 1 and no sub-cluster includes events which occur within particular time periods only. Therefore, we have also good indications that most events in Class 1 are indeed related to same glacial process over the year, which based on the ground truth data seems to be calving. However, we cannot fully exclude the possibility

that other processes or local seismic sources could be entrapped in our proxy for glacier calving due to the limitations of our data set and low matching rate with directly observed calving. The relationship between the calving process and glacier dynamics at Kronebreen which we discuss in Sect. 5.5 is therefore based on a hypothesis which has to be validated in future studies.

5.4 Temporal patterns in glacier-related seismicity

Assuming that seismic signals are generated by the same (glacial) processes over the year, we detect 7850 events within the entire seismic measurement period, among which 792 belong to Class 1. Seismic activity seems to be generally higher in 2009 compared to 2010 (Fig. 6). Even though comparison between absolute event rates in both years might be biased due to a slight change in location and coupling of the instrument, lower seismicity in 2010 is consistent with the number of direct visual observations. In 2009, 463 events have been counted per day on average, whereas in 2010 it was clearly less with 256 events per day. In both years seismic activity associated with Class 1 events seems to be higher in autumn than in the summer months. Increased seismicity in late summer has been observed previously for calving-related seismic events (O'Neel et al., 2010) and glacial earthquakes (Nettles and Ekström, 2010), and therefore seems to confirm the glacial origin of our detections.

The general seasonal trend is overlaid by short-term patterns of periods of 10 to 15 days in both years. For Class 1 events several peaks in the event rate in July 2009 are observed. There are pronounced peaks in event rate in May and in beginning of August for Class 1 events in 2010. However, the event rate may be affected by changes in background seismic noise level. We therefore compute the noise level as the RMS of seismic amplitudes 20 s before each detection onset and then averaged over one day intervals (see Fig. 6). At least one minimum in event activity in July 2009 coincides with one of three short peaks in the seismic noise level. Therefore, it is not clear at this time whether simply less events are detected on the geophone or less signals are emitted by the glacier. In 2010, the noise level is more stable besides one peak in the beginning of May (Fig. 6b). The noise level seems to increase slightly in summer 2010 which could be a result of decreasing burial depth of the geophone or continuous emitted noise of melt water. On average however noise levels are very similar in 2009 and 2010 which is an indication that the difference in observed seismicity in both years is mainly due to changing glacier activity.

5.5 Relationship between calving process and glacier dynamics

Recent thinning, acceleration and retreat of tidewater in different parts of the world raises the question of the relationship between calving processes and glacier dynamics (e.g.

Benn et al., 2007; Amundson and Truffer, 2010). To investigate the relationship between glacier speed and calving-related seismicity on seasonal time-scales, we analyzed qualitatively the three datasets available for 2009 and 2010: indirect measurement of iceberg calving (counts from seismic monitoring), glacier velocity (GPS measurements) and front positions (photogrammetry). In Fig. 6 the front position is indicated by a relative position compared to the first day of observations in spring 2009 and 2010. Furthermore, the change in front position is shown (first derivative). A positive front position indicates advance and negative retreat of the front with respect to the reference date. The solid green line represents the average position of the entire front while the dashed green line represents the front position only in Zone 1. We generate a timeline of the processes described above in an attempt to understand the relation between velocity, front position and calving-related seismicity.

For 2009 (Fig. 6a), the glacier speed is rather constant during the spring with acceleration beginning in mid-June, several peaks during the summer and deceleration at the end of July. Velocity remains more or less constant during the entire autumn except a peak at the end of August caused by a large rain event. The calving-related seismicity, represented by the seismic Class 1 events, remains low during the summer with three peaks that are more or less synchronous with the glacier speed peaks. During the autumn, our proxy for calving activity is about three times larger than during the summer. Finally, the glacier front slowly advances during the spring, reaching a plateau at the beginning of July when the front advance is at its maximum. The front remains rather constant all summer and starts retreating at the mid to end of July until the end of September (end of our photographic dataset). The relative change in front position is positive only during spring, it then becomes zero until the beginning of July and then negative until the end of September. During the winter months between October 2009 and May 2010, the front position advanced as observed in the field (no photographic dataset).

In 2010 (Fig. 6b), glacier speed begins increasing in mid-May until a maximum is reached at the end of June, followed by a short decrease and another maximum at the end of July before decreasing drastically until mid-August where it reaches another smaller maximum and finally decreases until the end of September. The calving-related seismicity remains low during the spring and the summer apart for two maxima, one mid-May and one at the beginning of August. The last one correlates well with an increase in velocity. At the end of August calving-related seismicity is increasing and staying at a higher level than during summer until the end of October. Finally the glacier position behaves differently than in 2009 with a fast and constant advance from mid-April until the middle or end of July, immediately followed by a continual retreat from later July until the end of October. The change in front position is mostly positive until mid-July, is zero for a few weeks and then becomes negative until mid-November.

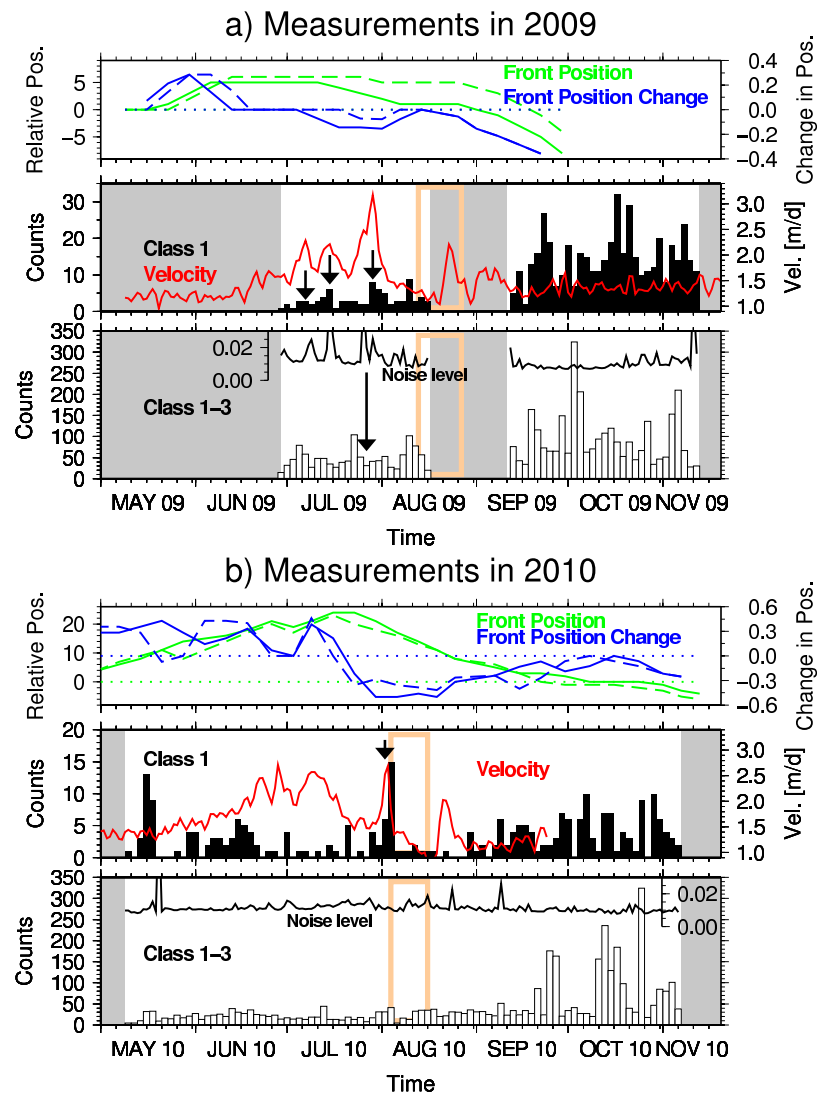


Fig. 6. (a) Lower panel: temporal distribution of seismic detections belonging to event classes 1 to 3 in 2009. Noise level in seismic data is shown using amplitude units in Volt. Grey areas represent data gaps and orange boxes periods of direct (visual) calving observations. Middle panel: same for Class 1 only (seismic events related to iceberg calving). Red curve shows velocity of Kronebreen measured close to calving front. Arrows indicate short-term correlations between GPS velocity, noise level, and event rate. Upper panel: green curve represents average, relative position and blue curve change in front position of entire front. Dashed lines indicate front position and change only in Zone 1. Horizontal, green-dotted curve shows position at first day of measurement in spring for each year and blue-dotted curve no change in front position (zero). Between October 2009 and May 2010, front position advanced as observed in field and from images. Note that zero reference in top panel of (a) and (b) vary between years. Positive values correspond to advance and negative to retreat of front. (b) Same as in (a) for 2010. Scale for Class 1 counts is different for 2009 and 2010.

From the two reconstructed timelines we can identify some patterns in the timing of the glacier dynamic events. Seismicity as a proxy for iceberg calving remains relatively low from May until mid-September while both velocity and front position undergo large fluctuations. For both years, calving-related seismicity increases in the autumn, when velocity is low and relatively constant but the front is retreating. Changes in velocity do not affect the seasonal fluctuations observed in calving-related seismicity, namely low

activity during spring and summer and increased activity from September on. On the other hand, short-term changes in velocity might affect small, weekly variations observed in calving-related seismicity, with an increase of iceberg discharge when velocity increases, as in the case in spring 2009 and early August 2010. This is consistent with theory connecting velocity changes and melt water pulse magnitudes (Schoof, 2010).

On seasonal time-scales, the calving process seems not to follow the typical seasonal velocity variation of the glacier. Calving-related seismicity shows a marked increase in the autumn (also observed in Alaska by O'Neel et al., 2010), which is accompanied by a continuous retreat of the glacier front. This suggests that our seasonal proxy for the calving rate is most likely influenced by a combination of different factors (e.g. 1st and 2nd order controls, Benn et al., 2007) as suggested in other recent studies (Amundson and Truffer, 2010; O'Neel et al., 2010) and not solely velocity. Velocity and calving-related seismicity are obviously linked, but through intermediate processes like stretching rate that favors the opening of crevasses (Venteris et al., 1997), basal velocity that influences basal conditions, crevasse deepening due to melt water at the glacier surface (O'Neel et al., 2003; O'Neel and Pfeffer, 2007), buoyancy perturbations (Warren et al., 1995; O'Neel et al., 2003; O'Neel and Pfeffer, 2007), front destabilization due to changes in the front geometry (Reeh, 1968; Hanson and Hooke, 2003), ocean temperature changes (Holland et al., 2008; Amundson et al., 2010) or preceding calving activity (Chapuis and Tetzlaff, 2012). All those processes may lead to a more unstable glacier front more susceptible to calving.

6 Conclusions

We have analyzed seismic data and direct visual observations of calving events at the terminus of Kronebreen, Svalbard. We have applied a traditional STA/LTA trigger algorithm with a very sensitive setting to detect all potential seismic signals emitted by glacial activity. The signals of all detections have been clustered to distinguish between different types of events and false detections using features that describe the temporal and amplitude characteristics as well as the frequency content of a seismic event. For clustering and identification of event clusters the Self-Organizing Map method has been used which simplifies visualizations of multi-dimensional data. We found that SOMs are particularly useful for geophone data which limit the use of a single event characteristic such as frequency content.

By comparing ground-truth data from the calving front with the obtained seismic detections, we were able to match ~10% of close calving events (<1 km from the geophone) with seismic signals. In combination with visual inspection of detections from all clusters, this allowed us to define three classes of seismic events. One class was interpreted to be related to calving (Class 1) and two others, with different degrees of uncertainty, to glacier activity in general (Class 2 and 3). Class 1 and 2 seismic events share similarities in length and frequency content with previously described event classes at glaciers, i.e. calving and fracturing. We have found that we were not able to monitor the entire calving front and to detect all events due to the noise level in the seismic data and limited instrumental sensitivity.

Beyond the time of direct observations, about 7850 seismic events are detected in total during several months in 2009 and 2010, including signals due to calving and probably also signals emitted by other sources in the glacier. Class 1 events which were interpreted to be related to calving activity suggests about 790 larger calving events in the vicinity of the seismic instrument. Temporal patterns in the event rate are found that reveal seasonal changes, i.e. increasing seismicity in autumn.

Using the subset of detectable seismic events as a proxy for calving activity at the glacier front, we analyzed the relationship between glacier velocity, front position and calving rate. Higher calving-related seismicity is found in autumn compared to the summer. Considering short-term variations, the seismic event rate is at least partially correlated with patterns in the ice flow velocity measured close to the glacier front with some peaks in velocity corresponding to small peaks in calving-related seismicity. However, on a seasonal time-scale, velocity and rate of seismic events due to calving seem to behave rather independently: in the autumn we observe an increase in calving-related seismicity while velocity is constant and low compared to the summer months. On seasonal time-scales, iceberg calving might therefore be partially controlled by other glacier dynamical processes.

Our results show the capability of monitoring glacier activity with seismic receivers to extend observational data sets and to obtain new insights about glacier dynamics. We found that a single-channel geophone, although limited by its sensitivity, can deliver useful information about calving activity. Improving the autonomous classification of calving-related seismicity will benefit from more than one instrument to determine the location of seismic sources at the glacier as well as more sensitive instrumentation (e.g. broadband receivers) allowing deeper investigation into the seismic characteristics of glacier induced signals. Finally, autonomous clustering and visualization using SOMs is a powerful technique providing immense potential to glacier-seismic analysis and future development of autonomous glacier-seismic monitoring systems (e.g. O'Neel et al., 2010).

Acknowledgements. We appreciate the very constructive reviews of Jason Amundson, Shad O'Neel, and Fabian Walter which helped to improve this manuscript. The calving observation project was supported by the IPY-GLACIODYN project (176076) funded by the Research Council of Norway (NFR). Fieldwork was made possible thanks to the Svalbard Science Forum funding (NFR). We would also like to thank Allan Buras, Bas Altena, Karin Amby, Damien Isambert and Mari Svanem for their great work observing the glacier in the field and Mats Björkman for field help installing the seismic instruments. Special thanks go to Tobias Baumann for the implementation of the STA/LTA trigger algorithm. Figures have been generated using the SOM toolbox (Vesanto et al., 2000) and the Generic Mapping Tools (Wessel and Smith, 1998).

Edited by: S. Marshall

References

- Allen, R. V.: Automatic earthquake recognition and timing from single traces, *B. Seismol. Soc. Am.*, 68, 1521–1532, 1978.
- Amundson, J. M. and Truffer, M.: A unifying framework for iceberg-calving models, *J. Glaciol.*, 56, 822–830, doi:10.3189/002214310794457173, 2010.
- Amundson, J. M., Truffer, M., Lüthi, M. P., Fahnestock, M., West, M., and Motyka, R. J.: Glacier, fjord, and seismic response to recent large calving events, Jakobshavn Isbræ, Greenland, *Geophys. Res. Lett.*, 35, L22501, doi:10.1029/2008GL035281, 2008.
- Amundson, J. M., Fahnestock, M., Truffer, M., Brown, J., Lüthi, M. P., and Motyka, R. J.: Ice mélange dynamics and implications for terminus stability, Jakobshavn Isbræ, Greenland, *J. Geophys. Res.*, 115, F01005, doi:10.1029/2009JF001405, 2010.
- Anandakrishnan, S. and Bentley, C. R.: Micro-earthquakes beneath Ice Streams Band C, West Antarctica: observations and implications, *J. Glaciol.*, 39, 455–462, 1993.
- Bardainne, T., Gaillot, P., Dubos-Sallée, N., Blanco, J., and Sénéchal, G.: Characterization of seismic waveforms and classification of seismic events using chirplet atomic decomposition. Example from the Lacq gas field (Western Pyrenees, France), *Geophys. J. Int.*, 166, 699–718, doi:10.1111/j.1365-246X.2006.03023.x, 2006.
- Benn, D. I., Warren, C. R., and Mottram, R. H.: Calving processes and the dynamics of calving glaciers, *Earth-Sci. Rev.*, 82, 143–179, doi:10.1016/j.earscirev.2007.02.002, 2007.
- Blankenship, D. D., Anandakrishnan, S., Kempf, J. L., and Bentley, C. R.: Microearthquakes under and alongside Ice Stream B, Antarctica, detected by a new passive seismic array, *Ann. Glaciol.*, 9, 30–34, 1987.
- Chapuis, A.: What controls the calving of glaciers? From observations to predictions, PhD thesis, Norwegian University of Life Sciences, Norway, 1–104, 2011.
- Chapuis, A. and Tetzlaff, T.: The variability of tidewater-glacier calving: origin of event-size and interval distributions, *J. Glaciol.*, in review, 2012.
- Chapuis, A., Rolstad, C., and Norland, R.: Interpretation of amplitude data from a ground-based radar in combination with terrestrial photogrammetry and visual observations for calving monitoring of Kronebreen, Svalbard, *Ann. Glaciol.*, 51, 34–40, doi:10.3189/172756410791392781, 2010.
- Davies, D. L. and Bouldin, D. W.: A cluster separation measure, *IEEE T. Pattern Anal.*, 1, 224–227, doi:10.1109/TPAMI.1979.4766909, 1979.
- Deichmann, N., Ansgore, J., Scherbaum, F., Aschwanden, A., Bernardi, F., and Gudmundsson, G. H.: Evidence for deep icequakes in an Alpine glacier, *Ann. Glaciol.*, 31, 85–90, doi:10.3189/172756400781820462, 2000.
- den Ouden, M. A. G., Reijmer, C. H., Pohjola, V., van de Wal, R. S. W., Oerlemans, J., and Boot, W.: Stand-alone single-frequency GPS ice velocity observations on Nordenskiöldbreen, Svalbard, *The Cryosphere*, 4, 593–604, doi:10.5194/tc-4-593-2010, 2010.
- Dowla, F. U., Taylor, S. R., and Anderson, R. W.: Seismic discrimination with artificial neural networks: preliminary results with regional spectral data, *B. Seismol. Soc. Am.*, 80, 1346–1373, 1990.
- Ekström, G., Nettles, M., and Abers, G. A.: Glacial earthquakes, *Science*, 302, 622–624, doi:10.1126/science.1088057, 2003.
- Esposito, A. M., Giudicepietro, F., D’Auria, L., Scarpetta, S., Martini, M. G., Coltelli, M., and Marinaro, M.: Unsupervised neural analysis of very-long-period events at Stromboli volcano using the self-organizing maps, *B. Seismol. Soc. Am.*, 98, 2449–2459, doi:10.1785/0120070110, 2008.
- Hanson, B. and Hooke, R.: Buckling rate and overhang development at a calving face, *J. Glaciol.*, 49, 577–586, doi:10.3189/172756503781830476, 2003.
- Holland, D., Thomas, R., De Young, B., Ribergaard, M., and Lyberth, B.: Acceleration of Jakobshavn Isbræ triggered by warm subsurface ocean waters, *Nat. Geosci.*, 1, 659–664, doi:10.1038/ngeo316, 2008.
- Jain, A.: Data clustering: 50 years beyond K-means, *Pattern Recogn. Lett.*, 31, 651–666, doi:10.1016/j.patrec.2009.09.011, 2010.
- Joswig, M.: Pattern recognition for earthquake detection, *B. Seismol. Soc. Am.*, 80, 170–186, 1990.
- Kääb, A., Lefauconnier, B., and Melvold, K.: Flow field of Kronebreen, Svalbard, using repeated Landsat 7 and ASTER data, *Ann. Glaciol.*, 42, 7–13, doi:10.3189/172756405781812916, 2005.
- Köhler, A., Ohrnberger, M., and Scherbaum, F.: Unsupervised feature selection and general pattern discovery using Self-Organizing Maps for gaining insights into the nature of seismic wavefields, *Comput. Geosci.*, 35, 1757–1767, doi:10.1016/j.cageo.2009.02.004, 2009.
- Köhler, A., Ohrnberger, M., and Scherbaum, F.: Unsupervised pattern recognition in continuous seismic wavefield records using Self-Organizing Maps, *Geophys. J. Int.*, 182, 1619–1630, doi:10.1111/j.1365-246X.2010.04709.x, 2010.
- Kohonen, T.: Self-Organizing Maps, Vol. 30 of Springer Series in Information Sciences, 3 extended Edn., Springer, Berlin, Heidelberg, New York, 2001.
- Maurer, W. J., Dowla, F. U., and Jarpe, S. P.: Seismic event interpretation using self-organizing neural networks, *Proceedings of the SPIE – The International Society for Optical Engineering*, 1709, 950–958, doi:10.1117/12.139971, 1992.
- Musil, M. and Plešinger, A.: Discrimination between local microearthquakes and quarry blasts by multi-layer perceptrons and Kohonen maps, *B. Seismol. Soc. Am.*, 86, 1077–1090, 1996.
- Nettles, M. and Ekström, G.: Glacial earthquakes in Greenland and Antarctica, *Annu. Rev. Earth Pl. Sc.*, 38, 467–491, doi:10.1146/annurev-earth-040809-152414, 2010.
- O’Neel, S. and Pfeffer, W. T.: Source mechanics for monochromatic icequakes produced during iceberg calving at Columbia Glacier, AK, *Geophys. Res. Lett.*, 34, L22502, doi:10.1029/2007GL031370, 2007.
- O’Neel, S., Echelmeyer, K. A., and Motyka, R. J.: Short-term variations in calving of a tidewater glacier: LeConte Glacier, Alaska, USA, *J. Glaciol.*, 49, 587–598, doi:10.3189/172756503781830430, 2003.
- O’Neel, S., Marshall, H. P., McNamara, D. E., and Pfeffer, W. T.: Seismic detection and analysis of icequakes at Columbia Glacier, Alaska, *J. Geophys. Res.*, 112, F03S23, doi:10.1029/2006JF000595, 2007.
- O’Neel, S., Larsen, C., Rupert, N., and Hansen, R.: Iceberg calving as a primary source of regional-scale glacier-generated seismicity in the St. Elias Mountains, *J. Geophys. Res.*, 115, F04034, doi:10.1029/2009JF001598, 2010.

- Pfeffer, W., Harper, J., and O'Neel, S.: Kinematic constraints on glacier contributions to 21st-century sea-level rise, *Science*, 321, 1340–1343, doi:10.1126/science.1159099, 2008.
- Plešinger, A., Růžek, B., and Boušková, A.: Statistical interpretation of WEBNET seismograms by artificial neural nets, *Stud. Geophys. Geod.*, 44, 251–271, doi:10.1023/A:1022119011057, 2000.
- Qamar, A.: Calving icebergs: a source of low-frequency seismic signals from Columbia Glacier, Alaska, *J. Geophys. Res.*, 93, 6615–6623, doi:10.1029/JB093iB06p06615, 1988.
- Reeh, N.: On the calving of ice from floating glaciers and ice shelves, *J. Glaciol.*, 7, 215–232, 1968.
- Richardson, J. P., Waite, G. P., FitzGerald, K. A., and Pennington, W. D.: Characteristics of seismic and acoustic signals produced by calving, Bering Glacier, Alaska, *Geophys. Res. Lett.*, 37, L03503, doi:10.1029/2009GL041113, 2010.
- Rolstad, C. and Norland, R.: Ground-based interferometric radar for velocity and calving-rate measurements of the tidewater glacier at Kronebreen, Svalbard, *Ann. Glaciol.*, 50, 47–54, doi:10.3189/172756409787769771, 2009.
- Schoof, C.: Ice-sheet acceleration driven by melt supply variability, *Nature*, 468, 803–806, doi:10.1038/nature09618, 2010.
- Stuart, G., Murray, T., Brisbourne, A., Styles, P., and Toon, S.: Seismic emissions from a surging glacier: Bakaninbreen, Svalbard, *Ann. Glaciol.*, 42, 151–157, doi:10.3189/172756405781812538, 2005.
- Taner, M., Koehler, F., and Sheriff, R.: Complex seismic trace analysis, *Geophysics*, 44, 1041–1063, doi:10.1190/1.1440994, 1979.
- Tarvainen, M.: Recognizing explosion sites with a self-organizing network for unsupervised learning, *Phys. Earth Planet. In.*, 113, 143–154, doi:10.1016/S0031-9201(99)00019-9, 1999.
- van der Veen, C. J.: Calving Glaciers: Report of a Workshop February 28–March 2, 1997, Tech. rep., BPRC Report No. 15, Byrd Polar Research Center, The Ohio State University, Columbus, Ohio, 1997.
- Vanwormer, D. and Berg, E.: Seismic evidence for glacier motion, *J. Glaciol.*, 12, 259–265, 1973.
- Venteris, E. R., Whillans, I. M., and van der Veen, C. J.: Effect of extension rate on terminus position, Columbia Glacier, Alaska, USA, *Ann. Glaciol.*, 24, 49–53, 1997.
- Vesanto, J. and Alhoniemi, E.: Clustering of the self-organizing map, *IEEE T. Neural Networ.*, 11, 586–600, doi:10.1109/72.846731, 2000.
- Vesanto, J., Himberg, J., Alhoniemi, E., and Parhankangas, J.: SOM toolbox for Matlab, Tech. rep., Helsinki University of Technology, Helsinki, 2000.
- Wald, A. and Wolfowitz, J.: On a test whether two samples are from the same population, *Ann. Math. Stat.*, 11, 147–162, doi:10.1214/aoms/1177731909, 1940.
- Walsh, K. M., Howat, I. M., Ahn, Y., and Enderlin, E. M.: Changes in the marine-terminating glaciers of central east Greenland, 2000–2010, *The Cryosphere*, 6, 211–220, doi:10.5194/tc-6-211-2012, 2012.
- Walter, F., O'Neel, S., McNamara, D., Pfeffer, W., Bassis, J., and Fricker, H.: Iceberg calving during transition from grounded to floating ice: Columbia Glacier, Alaska, *Geophys. Res. Lett.*, 37, L15501, doi:10.1029/2010GL043201, 2010.
- Warren, C. R., Glasser, N. F., Harrison, S., Winchester, V., Kerr, A. R., and Rivera, A.: Characteristics of tide-water calving at Glaciar San Rafael, Chile, *J. Glaciol.*, 41, 273–289, 1995.
- Washburn, B.: Exploring Yukon's glacial stronghold, *Natl. Geogr. Mag.*, 69, 715–748, 1936.
- Weaver, C. S. and Malone, S. D.: Seismic evidence for discrete glacier motion at the rock-ice interface, *J. Glaciol.*, 23, 171–184, 1979.
- Wessel, P. and Smith, W. H. F.: New, improved version of GMT released, *EOS T. Am. Geophys. Un.*, 79, 579–579, doi:10.1029/98EO00426, 1998.
- West, M., Larsen, C., Truffer, M., O'Neel, S., and LeBlanc, L.: Glacier microseismicity, *Geology*, 38, 319–322, doi:10.1130/G30606.1, 2010.
- Wolf, L. W. and Davies, J. N.: Glacier-generated earthquakes from Prince William Sound, Alaska, *B. Seismol. Soc. Am.*, 76, 367–379, 1986.